Evolving Earth 2 (2024) 100041

Contents lists available at ScienceDirect

Evolving Earth

journal homepage: www.sciencedirect.com/journal/evolving-earth

Morphometry and active tectonics of the Konkan coast, western India

Shatavisa Chatterjee [a], Kutubuddin Ansari [b], Mery Biswas [c], Soumyajit Mukherjee [a,*], B. Kavitha [d]

[a] Department of Earth Sciences, Indian Institute of Technology Bombay, Powai, Mumbai, 400 076, Maharashtra, India
[b] Integrated Geoinformation (IntGeo) Solution Private Limited, New Delhi, 110 025, India
[c] Department of Geography, Presidency University, 86/1 College Street, Kolkata, 700 073, West Bengal, India
[d] Department of Civil Engineering, National Institute of Technology Warangal, Telengana, 506 004, India

ARTICLE INFO

Keywords:
Linear and spatial morphometry
Tectonics
Regional deformation
Bouguer anomaly
B-value
Seismicity

ABSTRACT

The Indian western coast is petroliferous and draws attention from academicians and industrial experts. In this work, geomorphic indices have been calculated to decode neotectonics of the Konkan onshore region on India's west coast. Earthquake and Bouguer anomaly data have been used along with the present-day stress data from the World Stress Map project. Gravity modeling was performed in order to gain seismotectonic insights. The b-values were determined using Z-MAP 7.1 (2021). Morphometric analysis at both linear and spatial scales were performed using the digital elevation model from the data derived from the Shuttle Radar Topography Mission, analyzed with ArcGIS 10.3 (2014) software. Maps depicting slopes, aspects, and reliefs were created. NW-SE trending lineaments in the Konkan plain guided the major stream courses. Two of the five watersheds, watersheds 4 and 5, reveal high tectonic activity, are landslide-prone and host hot springs. Interestingly, watersheds 4 and 5 show high b-values (except near the rivers' sources), low Bouguer anomalies, and higher Hypsometric integral values (0.18523 and 0.16698) than the other watersheds. A low b-value in watershed 3 indicates stress accumulation. Over a larger area, the gravity trend varies from ~ -80 to 30 mGal. The lineaments diagram deduced from the first vertical derivative technique shows that the structural fabrics mostly trend ~ NW-SE at the west of the Western Ghat Escarpment (WGE) while it is NE-SW at the east. The tilt derivative ratio technique reveals a major NE-SW trend to the west of the WGE and an E-W trend to the east. Structural interpretations based on drill-cores around Koyna combined with geophysical studies for deep crust will be required are required for a better understanding of the blind (active) structures in the region.

1. Introduction

Neotectonics is associated with areas of active seismicity and faulting. To study neotectonics evidence, geologists initially focussed only on tectonic landforms in field studies (e.g., Biswas et al., 2022). Recently, satellite imagery has been used widely to study these landforms (e.g., Gogoi et al., 2022, Biswas et al., 2022). Neotectonics is most commonly decoded through drainage system analysis (e.g., Dasgupta et al., 2022). While space-based geodesy can detect tectonic strain rates of the order of few μ strain/yr, fluvial systems and landforms can record strain rates that are up to ten times slower, i.e., ~0.1 μ strain/yr (Kannaujiya et al., 2022). Fluvial landforms also record episodic and cyclic palaeo-activities, making the changing fluvial systems and drainage patterns excellent indicators of ongoing tectonic processes. These changes can be quantified using geomorphic indices (Keller, 1986; Keller and Pinter, 2002). According to Zhou et al. (2022), recent trends in tectonic geomorphology research emphasize the analysis of landform evolution by constraining the rate of active tectonics using remote sensing data.

The Koyna-Warna seismic zone falls within the seismic zone IV on the seismic zonation map of India (Chenna et al., 2010). In 1967, the Koyna-Warna region experienced an earthquake of magnitude 6.3, which is the largest recorded case of reservoir-induced seismicity in India (Singh et al., 2008). Kaila et al. (1981) geophysically documented deep faults, one of which was presumably related to the Koyna earthquake. Seismicity in the Koyna-Warna region is confined to 11 km × 16 km area and within 3-9 km depth (Rai and Saha 2024). Clay mineralization along brittle planes can be attributed to the repeated nature of seismicity in the region (Haldar et al. 2024). The Koyna seismic zone is divided into three sub-zones: North Escarpment Zone (NEZ), South

* Corresponding author.
E-mail addresses: soumyajitm@gmail.com, smukherjee@iitb.ac.in (S. Mukherjee).

https://doi.org/10.1016/j.eve.2024.100041
Received 28 July 2024; Received in revised form 10 October 2024; Accepted 14 October 2024
Available online 21 October 2024
2950-1172/© 2024 The Author(s). Published by Elsevier Ltd. This is an open access article under the CC BY license (http://creativecommons.org/licenses/by/4.0/).

Escarpment Zone (SEZ), and Warna Seismic Zone (WSZ) (Fig. 1) (Rai et al., 1999). Earthquakes are generated primarily by normal and strike-slip faults and are confined mainly to the downstream region of the Koyna River (Singh et al., 2008).

The high extensional stress accumulation over the western coastal region is attributed to the flexure of the western boundary of the Indian plate and the reservoir-induced strain accumulation near the Koyna region (Kom and Singh, 2016). Fractures in the Koyna region's basalts in the Koyna region extend deep into the basement creating pathways for water percolation and increasing seismicity potential in the area (Modak, 2024). The Global Positioning System (GPS) station installed at the Indian Institute of Technology Bombay (Powai, Mumbai) shows a velocity residual of 9.91 mm yr^{-1} toward the southwest under an India-fixed condition, which is more than other regions in the Indian plate. This strain accumulation in the region may cause earthquakes and other natural hazards (Kom and Singh, 2016).

The study area for this work is located between the Western Ghats/Sahayadri and the Arabian Sea. The Western Ghats have been considered a shoulder of passive rifting between India and Madagascar (Gunnell and Fleitout, 2000). The region partially overlaps the Konkan coast in the Deccan plateau-a sub-province of the Deccan traps.

This work aims to *(i)* demarcate tectonically active areas in the Konkan coastal region, and *(ii)* perform lineament analyses to decipher the tectonics. To achieve this, we utilize secondary data throughout the study. Watersheds of the five major ~ west-flowing rivers are demarcated (Fig. 1). Tectonic instability of the study region is investigated by calculating the morphometric parameters on both linear and basin scales. Additionally, we analyze the Bouguer anomaly variation and the b-value of the region to establish a correlation with the morphometric analysis. We performed several analyses and compiled data from the

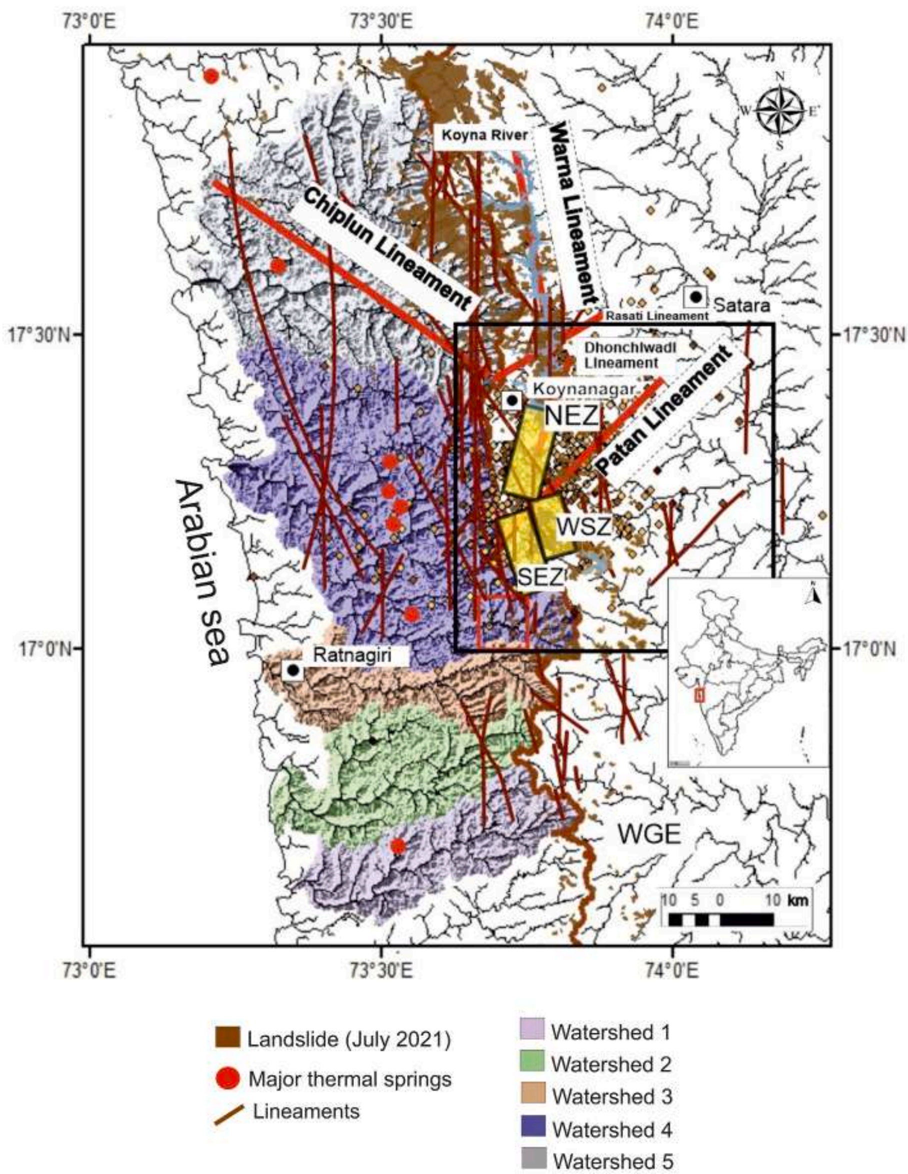

Fig. 1. Geoscientific aspects of the study area (detail in Repository Fig. 1). Red rectangle in inset map of India is the study area. Earthquake prone region and major lineaments are five major rivers- Vaghotan (in watershed 1), Muchkundi (in watershed 2), Kajali (in watershed 3), Jaigad (in watershed 4) and Vashisthi (in watershed 5) and their watersheds are marked in different colours. Red box in the main figure: zone susceptible to landslides (Internet ref-1). Brown patches: landslide data taken from BHUVAN (https://bhuvan.nrsc.gov.in/home/index.php). NEZ: North Escarpment Zone; SEZ: South Escarpment Zone; WGE: Western Ghat Escarpment; WSZ: Warna Seismic Zone and the Koyna–Warna Fault plotted from Arora and Srinu (2022). A Bouguer anomaly map (Fig. 8) has been prepared for the area within the black rectangle. (For interpretation of the references to colour in this figure legend, the reader is referred to the Web version of this article.)

literature to cross-check the active tectonics of the delineated areas. Applying multiple techniques to address a single problem and assessing consistency and confirmation of results, is a standard process in (geo) scientific research (e.g., Vanik et al., 2018). Further, through gravity modeling, we deduced lineaments in the area. Analysis revealed the edge locations of lineaments at zero amplitudes for the vertical source. The estimated parameters are able to provide low and rounded amplitudes for deeper sources as well as high and sharp amplitudes at shallower depths.

Previous studies focused on the geomorphology of the Konkan area (e.g., Dikshit, 1976). Jadhav and Kshirsagar (2017) and Arora and Srinu (2021), for example, performed morphometric studies, but were restricted to the Koyna region, making it impossible to compare the tectonic activeness of the Koyna area with the nearby areas of Konkan region. A comprehensive morphometric study incorporating additional tectonic factors for the region remained a gap in the literature.

Being adjacent to two hydrocarbon-bearing basins to its NNW- the Bombay/Mumbai offshore and the Cambay basin, both onshore and offshore of the Konkan basin has also been studied for hydrocarbon exploration. For example, oil and gas shows were found in the Kerala-Konkan shelf through 14 exploratory wells (Kumar 2018), and the shelf area was classified as a Category III basin (Dwivedi, 2016). The presence of well-defined structural elements, reservoir facies, and probable source rocks make the Konkan basin potential prospect for hydrocarbons (Singh and Lal, 2001).

Although the present study focuses on the onshore Konkan region, knowledge of tectonic activity will be crucial for addressing wellbore stability issue in future onshore drilling operations are made. Identifying areas with active tectonics is essential for ensuring the stability of drilled wells. Stress conditions are also required for reservoir modeling in the exploration stage. The seismotectonic analysis performed in this study provides insights into the accumulated stress in the region (e.g., Lavecchia et al., 2021).

2. Geological background

2.1. Lithology

The Konkan plain, below the escarpment, is covered by a lateritic cap that is younger than the laterite atop the plateau. The Konkan laterites are termed the “low-level laterites” while those on the uplands are the “high-level laterites”. The former were formed by the removal of the more mobile elements due to the action of groundwater (Widdowson and Cox, 1996). The laterites found in the study area evolved from the Ambenali (plotted in Fig. 1) and Poladpur (located in Fig. 1) rocks on which the laterites reside. Paleomagnetic evidences indicate that the development of the laterite from the Panhala rocks occurred during the Mid-Tertiary when substantial erosion took place. Holocene sediments along the Ratnagiri coast consists of a mixture of fine to coarse sand and clay (Sahasrabudhe 1999).

2.2. Geomorphology

The erosional retreat of the so-called West Coast Fault due to the rifting of the Indian plate formed the Konkan coastal belt. Alternately, an eastward tilt of the Indian plate produced this belt (review by Jain et al., 2020).

In the eastern part, the Sahyadri/Western Ghat ranges are gentler and merge gradually into the peninsular Deccan plateau (Kumar et al., 2022). Although about half of the range consists of Precambrian rocks, the uplift of these ranges is primarily linked to the Cenozoic evolution of the western continental margin of India (WCMI; Jain et al., 2020). The western part of the Western Ghat is designated as the Konkan Coastal Belt (KCB). The southern KCB consists of sub-horizontal Deccan trap basaltic flows with extensive lateritic covers (Dessai and Bertrand, 1995). Rivers originating from the Western Ghat flow west towards the Arabian Sea (Jain et al., 2020), and have orthogonal tributaries (Kundu et al., 2000). These rivers show linear narrow channels with actively headward erosion, waterfalls and cascades. The eastern part of the Western Ghat escarpment is referred to as the Western Uplands. The KCB consists of several sub-parallel flat-topped ranges with NW-SE to WNW-ESE wide river valleys. KCB’s elevation gradually drops towards the east and merges with the plain (Kale et al., 2017).

Beaches along the southern Konkan coast are narrow and paired with (sub)vertical cliffs and flat rock beds. The Western Ghat Escarpment (WGE) acts as a drainage divide between the west and the east-flowing rivers. The rivers flowing west cross the Konkan coast and drain into the Arabian Sea, whereas the rivers flowing east drain into the Bay of Bengal across the Indian peninsula. Kale et al. (2017) suggested that the current morphometric setup can be explained by differential neotectonic uplift. The drainage system of the Deccan traps is modified by the Tertiary and Quaternary reactivations of the sub-Trappean discontinuities (Mukherjee et al., 2020).

The most prominent lineament in the area is the Western Ghat escarpment. It is marked by a sharp change in the topography and elevation, with the eastern side being elevated by 800–1200 m. The escarpment is considered a rift-bounding fault along the passive margin of the west coast (Mukherjee et al., 2017). The offshore graben along the western coast developed during the Eocene. The graben’s development was followed by the retreat of the Western Ghats scarp due to headward erosion by consequent streams (Radhakrishna, 1993). The Western Ghat formed a structurally-controlled escarpment that was modified due to geomorphic processes, e.g., scarp retreat and inland retreat across the evolving continental margin.

2.3. Igneous episodes, seismicity and structures

Lava flows in the study area mostly composed of basalts, with interspersed acidic mafic and ultramafic rocks (Rajaram et al., 2017). Eruptions occurred during both in the Late Cretaceous and Eocene-Oligocene (Mukherjee et al., 2017). Igneous rocks in the Western Ghats erupted presumably within 65-60 Ma (Beane et al., 1986). The study area includes N-S dyke swarms of basalts, dolerite lamprophyres, and alkaline rocks (Sheth, 2007).

Magnetotelluric studies in the Koyna-Warna Seismic zone conducted by Borah et al. (2023) revealed that the thickness of the trap is ~800 m overlying a fractured granitic basement. Around 26.5 MPa overburden pressure is exerted by the trap rock on the overburden (Borah et al., 2023). The Donchiwadi fracture/fault zone has been well identified in the Koyna region and was a result of the M 6.3 Koyna earthquake in 1967 (review in Modak et al., 2022; also see Arora and Srinu, 2022). Borehole geophysical surveys further revealed that the fracture zone at depth is water-filled (Podugu et al., 2023), indicating that the brittle planes can be susceptible to slip. Podugu et al. (2023) further speculated about existence of a blind fault system at depth. Shekar et al. (2023) deduced a high seismic parameter $\eta > 1$ from the Koyna-Warna zone, indicating its high potential for earthquakes. Seismicities in this region originated within 3–11 km depth (Sarma and Srinagesh 2007).

The Konkan coast represents the downthrown block of Western Ghat that formed presumably due to the presence or activation of the N-S trending fault during the Late Pliocene. The NNW-SSE striking Koyna fault runs parallel to the Western Ghat escarpment (Mukherjee et al., 2017). The basalts in the region and also the basement rocks have been subdivided into few layers based on geophysical properties. Rocks at ~ 10 km depth have been proved to be of significantly higher temperature (Ray et al., 2021). Non-parallelism between the fast polarization azimuth and SHmax at few places in the Koyna Warna region is probably related to surface topography (Roy and Shashidhar, 2023). Bhave et al. (2017) documented from the Koyna-Warna region NW trending reverse faults ("Sutarwadi Fault Zone"). The Warna lineament is associated with a fault in the Archean basement that activated after the Deccan volcanism event (Rajurkaret al.1990). The Kurduwadi Lineament and the

Peninsular lineament strike NW (Peshwa and Kale, 1997; Rajaram et al., 2010; 2017), which are ascribed to the uplift and rifting of the western passive continental margin (Subrahmanya and Syrnp, 1996). Several NW-SE trending faults/shear zones have been observed in the Konkan coast's southern part. These lineaments presumably run throughout the Deccan basalts, the laterite cover, and the basement rocks as well. The seismic activity near the Koyna-Warna region has been attributed to the NW-trending Chiplun Fault, which is a reactivated basement shear (Mukherjee et al., 2020).

3. Methodology

We approached active tectonic study from multiple perspectives. The aim was to determine whether these different techniques converge on the same conclusion. It is important to note that the same terrain may be classified as tectonically (in)active depending on the approach used. For instance, not all morphometric parameters necessarily indicate tectonic activity of a given terrain (e.g., Biswas et al., 2024). Secondly, the b-values can be sensitive indicators of tectonic activities; however, in exactly what way is debated (Gadkari and Mukherjee, 2023). Additionally, an earthquake can occur within a short time frame due to the stick-slip mechanism in a 3D rock volume, even where no morphometric anomalies have been detected. Furthermore, landslide susceptibility is influenced by factors beyond tectonic activity, including rainfall, lithology, slope and human activities. For active tectonic studies, therefore, multidisciplinary approaches are recommended (e.g., Bayasgalan et al., 2005). Refer to Shekar and Mathew (2024), Wiemer (2001), Hirata (1989), and Baratin et al. (2016) for the theories behind morphometry, map program, b-value, and gravity studies, respectively.

3.1. Linear aspects

3.1.1. Longitudinal profile analysis

Five rivers originating from the Western Ghat and flow into the Arabian Sea were selected and their watersheds were delineated (Fig. 1). Repository Fig. 2 presents watershed map superposed on lithologic map of the study area. Longitudinal profiles of these rivers are generated within a Geographic Information System (GIS) environment using the ArcGIS software. The data used originated from the Shuttle Radar Topography Mission Digital Elevation Model (SRTM DEM) published on 01-Oct-2012 with a resolution of 30 m × 30 m. A relief map (Fig. 2a) was created to visualize the morphology. Additionally, a slope map (Fig. 2b) and an aspect map (Fig. 2c) were generated to characterize the variation in slope and its directional orientation.

3.1.2. SL index

The SL index is used to identify regions that have undergone recent tectonic activity (Keller and Pinter, 2002). The formula is:

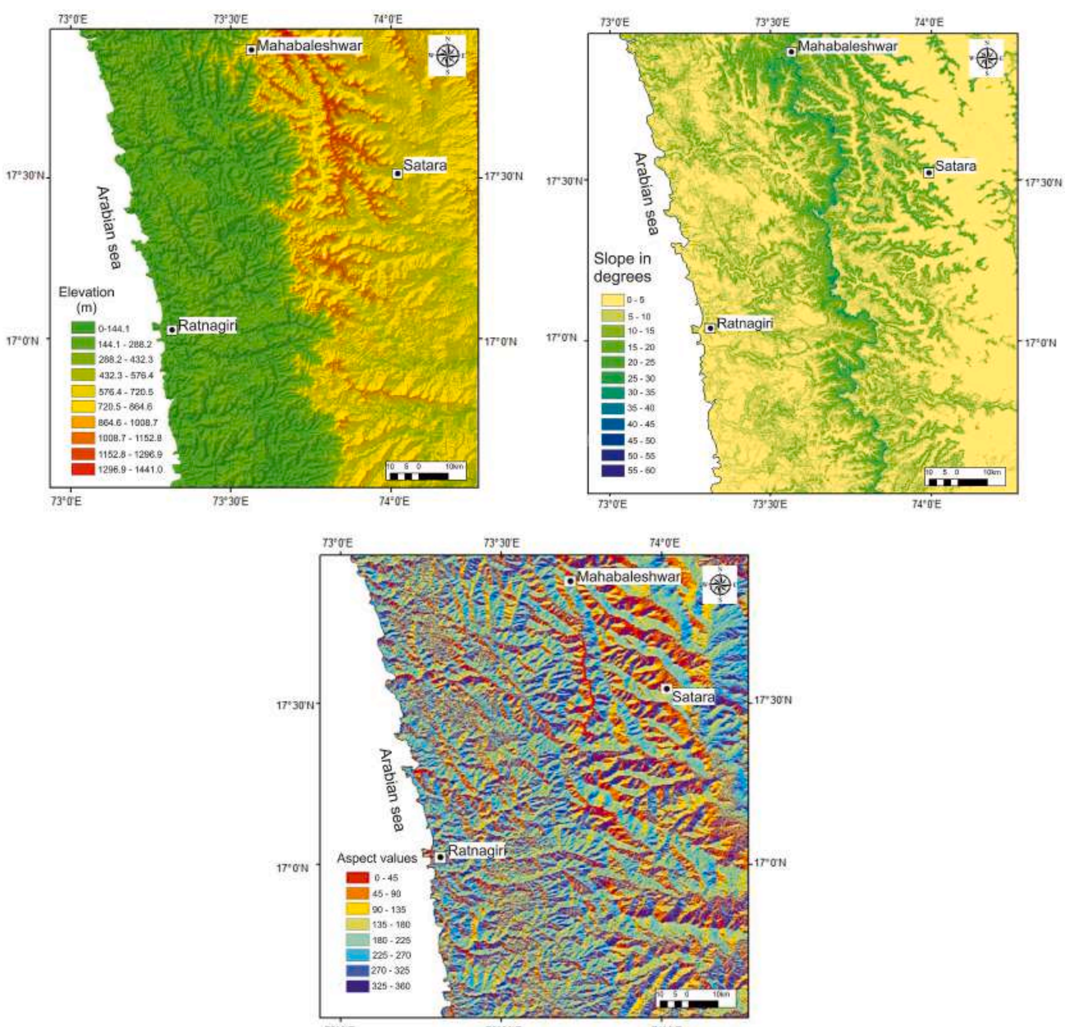

Fig. 2. a. Relief map of the study area- 2D view by incorporating slope and elevation. **b.** Slope map. Elevation presented. Red colour: steep slope denoting WGE. Major rivers identify sudden change in slope. **c.** Aspect map. Aspect values indicate the direction of the slope faces. 0: north, 90: east etc. (For interpretation of the references to colour in this figure legend, the reader is referred to the Web version of this article.)

$$SL = (\Delta H / \Delta L) * L \tag{1}$$

$\Delta H/\Delta L$: Slope of the river; L: Length of the river channel.

In this study, the main rivers in the different watersheds were divided into ~5 km segments along their lengths and the SL indices were calculated. The lengths of these rivers within the watersheds range from 65 to 105 km. Using longer segments would decrease the accuracy of the SL index, while shorter segments would make the calculation more time-consuming.

3.1.3. Sinuosity index (SI)

The elevation and distance were plotted on the Y and X axes, respectively, using the software Origin (2021). For each channel segment, the corresponding ratio of the channel (C) to valley (V) lengths was measured, and sinuosity was calculated using the formula (Mueller, 1968):

The five rivers in the study area have been delineated using Google Earth Pro and marked on

$$SI = C\ V^{-1} \tag{2}$$

3.1.4. Concavity index (θ)

The parameter describes the rate of change of the channel gradient towards the downstream of the river. The relationship between the gradient of the stream (S), concavity (θ), area of the basin (A), and steepness (k_s) is (Gailleton et al., 2021):

$$S = k_s . A^{-\theta} \tag{3}$$

It is calculated by plotting the logarithm of slope vs. the logarithm of area of the river. The slope of the regression line is the concavity index (Gailleton et al., 2021).

3.2. Areal aspects

3.2.1. Hypsometric analysis

The hypsometric curves for each watershed are generated by plotting the relative height of the basin against the relative area (e.g., Cheng et al., 2012, Cheng et al., 2012). The relative height ($h.H^{-1}$) is the proportion of the total basin height, and the relative area ($a.A^{-1}$) is the proportion of the total basin area. Here, H represents the difference between the maximum and minimum elevation within the basin, A is the total area of the basin, and a is the area within the basin above a certain elevation h. The hypsometric integral (HI) is determined by integrating the area under the curve using the Origin (2021) software.

3.2.2. Asymmetry factor (AF)

The asymmetry factor was calculated using the following formula (Keller and Pinter, 1996):

$$AF = \left(A_r . At^{-1}\right) * 100 \tag{4}$$

A_r: area of the basin towards the right of the main river channel, facing downstream, and A_t: the total area of the basin. In order to determine the AF, all the watershed areas are divided into two portions, the area left and right of the main channel, and eqn (4) is applied.

3.2.3. Mountain front sinuosity

It was calculated using the following formula (Keller and Pinter, 1996):

$$S_{mf} = L_{mf}\ L_s^{-1} \tag{5}$$

L_{mf}: curved distance of the mountain(/hill) along the front (in other words, curved length of the mountain that falls within the watershed). Here the two points are the intersections of the mountain range and the watershed boundary; L_s: straight distance.

3.2.4. Drainage texture

Drainage texture was calculated by using the following formula (Horton, 1945):

$$Rt = Nu\ P^{-1} \tag{6}$$

Rt: drainage texture; Nu: total number of streams of all orders; P: perimeter of the watershed.

3.2.5. Drainage density

Drainage density is obtained by using the following formula:

$$D = Lu\ A^{-1} \tag{7}$$

(Horton, 1932)D: drainage density; Lu: total stream length of all orders; A: area of the basin (km^2)

Drainage density measures the total length of the channel per unit area in a watershed. The higher the density, the more closely spaced the channels.

3.2.6. Basin shape index

Basin shape was calculated using the following formula (Schumm, 1956):

$$Bs = B1\ Bw^{-1} \tag{8}$$

B1: basin length; Bw: width of the basin measured at its widest part.

3.3. Seismotectonic analysis

3.3.1. World Stress Map

The data available from the World Stress Map (WSM) within the study area indicates normal and strike-slip faulting regimes (Fig. 3). The stress regimes are mainly derived from the earthquake focal mechanisms (Heidbach et al., 2019).

3.3.2. Bouguer anomaly map and earthquake distribution

The gravity data for the Bouguer anomaly map was taken from the Earth Gravitational Model (EGM2008: https://bgi.obs-mip.fr/data-products/outils/egm2008-anomaly-maps-visualization/) released by the

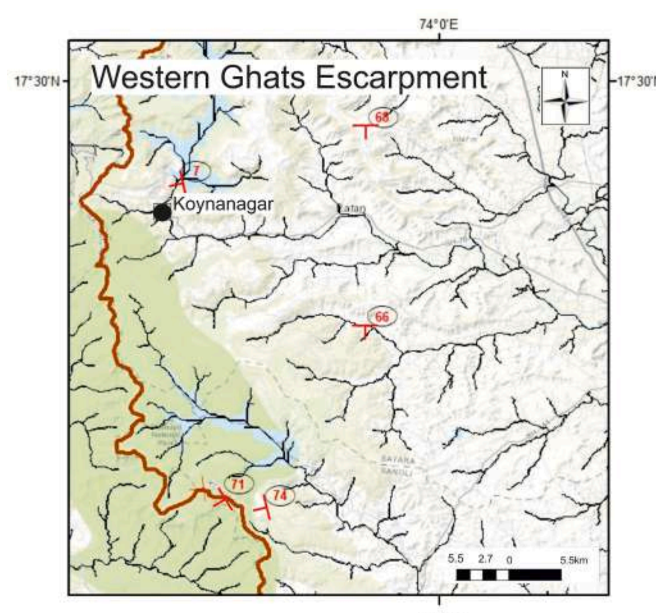

Fig. 3. Azimuth and plunge of the maximum horizontal stress direction as per the World Stress Map. Green: forest cover. (For interpretation of the references to colour in this figure legend, the reader is referred to the Web version of this article.)

National Geospatial-Intelligence Agency (NGA). The data from 1965 to 2021 were used in this work. The data was processed on ArcGIS 10.3 (2014), and the map was prepared in CorelDRAW 2007.

The empirical relation between the magnitude of earthquakes and their frequency of occurrence in a region is:

$$\text{Log N(M)} = (\text{a} - \text{b. M}) \tag{9}$$

Gutenberg and Richter 1954 N(M): annual number of earthquakes of Richter magnitude > M; a: measure of seismic activity over the region. b: rate of fall in the frequency of seismic events with increasing magnitude. ‘b’ < 1 indicates fewer earthquakes in a larger magnitude range. This can mean the possibility of large-magnitude earthquakes in the future (e.g., Gupta and Biswas, 2023).

3.3.3. Landslide susceptibility

Several presentations of landslide data from the Konkan area have been available (e.g., fig. 5c of Martha et al., 2021). According to the National Landslide Management Strategy (Sept 2019), the area bounded between 17°0′00″N to 17°0′05″N latitudes and 73°0′40″E to 73°0′ 45″E longitudes in the Ratnagiri District is more susceptible to landslides than the surrounding regions (Martha et al., 2021). This region falls within our delineated watershed 4, which is highly tectonically active. The data for the landslide for July 2021 (Internet ref-1) has been plotted in Fig. 1, west of the Warna Lineament. This shows that the maximum concentration of landslides took place in the region falling in and around watershed 5, which is also highly active tectonically. The data has been collected from the BHUVAN (Internet ref-2) maintained by the Indian Space Research Organisation.

3.4. Gravity modeling

The information about tectonic boundaries, gravity extension, and trends is commonly analyzed by two or more edge detection techniques (e.g., Pal et al., 2016; Kumar et al., 2022). These techniques estimate several gravity parameters commonly known as first vertical derivative (FVD), total horizontal derivative (THD), and tilt derivative ratio (TDR). The FVD is the vertical/depth-wise rate of change of gravity, while the THD is a parameter that can detect edges (Wu et al., 2017). These parameters provide low and rounded amplitudes for deeper sources as well as high and sharp amplitudes for shallower sources. The FVD reveals zero amplitudes at the edge locations for the vertical source and has been effectively implicated by several investigations (e.g., Pal et al., 2016; Ganguli et al., 2019; Horo et al., 2020; Kumar et al., 2022). This technique improves the responses from the source with shallower boundaries by controlling the regional responses. The FVD gravity anomaly (g_z) amplitudes with respect to the elevation height (z) are calculated as follows (Evjen, 1936):

$$FVD = \frac{\partial g_z}{\partial z} \tag{10}$$

The THD amplitude utilizes the x- and y-directional derivatives combined response and is computed as follows (Miller and Singh, 1994):

$$THD = \sqrt{\left(\frac{\partial g_z}{\partial x}\right)^2 + \left(\frac{\partial g_z}{\partial y}\right)^2} \tag{11}$$

The arctan ratio of FVD to THD amplitudes is known as TDR. It varies between $-\pi/2$ and $\pi/2$. The technique provides zero amplitudes at the vertical boundary sources over the source axis. TDR is estimated as follows (Miller and Singh, 1994):

$$TDR = \tan^{-1}\left(\frac{FVD}{THD}\right) \tag{12}$$

These enhancement techniques used first-order derivatives and several combined derivatives of the potential fields. Their results better enhance the anomalies. The techniques to can also provide linear, circular, and rectangular tectonic boundary enhancement at varying depths up to the Moho (Narayan et al., 2017; Kumar et al., 2022).

4. Results

4.1. Linear aspects

The longitudinal profiles of the five rivers (main channels) are presented in Fig. 4. Anomalies in the elevation vs. distance graph are indicated by red arrows. The profiles of most of them show a sharp drop in elevation, which corresponds to the knick-points (Fig. 4).

The SI values of the river segments were calculated, starting from the mouth of the river (Fig. 4). The values were divided into four classes, viz. 1–1.05 ⇒ straight channel, 1.05–1.5 ⇒ sinuous channel, 1.5–2 ⇒ meandering channel and >2 ⇒ braiding channel. These are represented by different colours on the longitudinal profiles. A sharp drop in SI is usually accompanied by an adjacent increase in SI. The lineaments that cut across the river and those parallel to the river are also marked on the profiles. The SL index values and concavity values of each segment are stated on the graphs as well (Fig. 4).

Table 1 presents the R^2 values of the trendline of the longitudinal profiles for the four watersheds. For the watersheds 1, 2 and 3, the logarithmic trendline shows the maximum values. For watersheds 4 and 5, the highest values fit the exponential curve. This indicates that main streams of watersheds 4 and 5 show high tectonic activity whereas main streams of watersheds 1, 2 and 3 are moderately active (e.g., Lee and Tsai, 2010).

4.2. Areal aspects

The hypsometric curves of all five watersheds are sigmoid (Fig. 5). The HI values are low but steadily increase from watersheds 1 to 5 (Table 2). Table 2 presents the AF values of the five watersheds, which vary from 37.14 to 79.29. Fig. 6 illustrates the tilt of the watersheds with the corresponding values provided in Table 2. The S_{mf} value steadily decreases from watersheds 1 to 5. Drainage texture, defined as the ratio of stream segments of all orders to the perimeter of the watershed, allows the classification of grains into five categories (Smith, 1950): very coarse (<2), coarse (2–4), moderate (4–6), fine (6–8), and very fine (>8). Although all five watersheds fall under the very coarse class (<2), watersheds 4 and 5 exhibited significantly higher values than those of watersheds 1–3. The drainage densities were nearly equal, with values of 0.361, 0.347, 0.332, 0.356 and 0.363. Since the drainage density values for the different watersheds in this study were nearly the same, this parameter did not play a significant role in active tectonics in this region. The lower the Bs values, the more circular the basin shape. Generally, an elongated basin correlates with tectonically active areas; however, in this case, the more circular watersheds (4 and 5) were also more active tectonically. This can be attributed to the fact that the drainage patterns in watersheds 4 and 5 are primarily lineament-controlled.

4.3. Seismotectonic analysis

Earthquake data (magnitude type) was considered for the study as provided in the USGS data catalog (https://earthquake.usgs.gov/earthquakes/search/). An earthquake’s magnitude is translated into seismic energy and follows a power-law distribution known as the Gutenberg-Richter (GR) law, which approximates the number of earthquakes with a magnitude exceeding M, or n(M) (Iwata and Nanjo, 2024). The magnitude frequency of earthquakes follows an exponential distribution. Z-Map 7.1, a program compatible with MATLAB 18 version, was used to handle and analyze the seismic data (Rehaman et al., 2015; Gupta and Biswas, 2023).

Regions where the earthquake data is available, i.e., partially in the watersheds 4 and 5, were divided into four sections covering equal

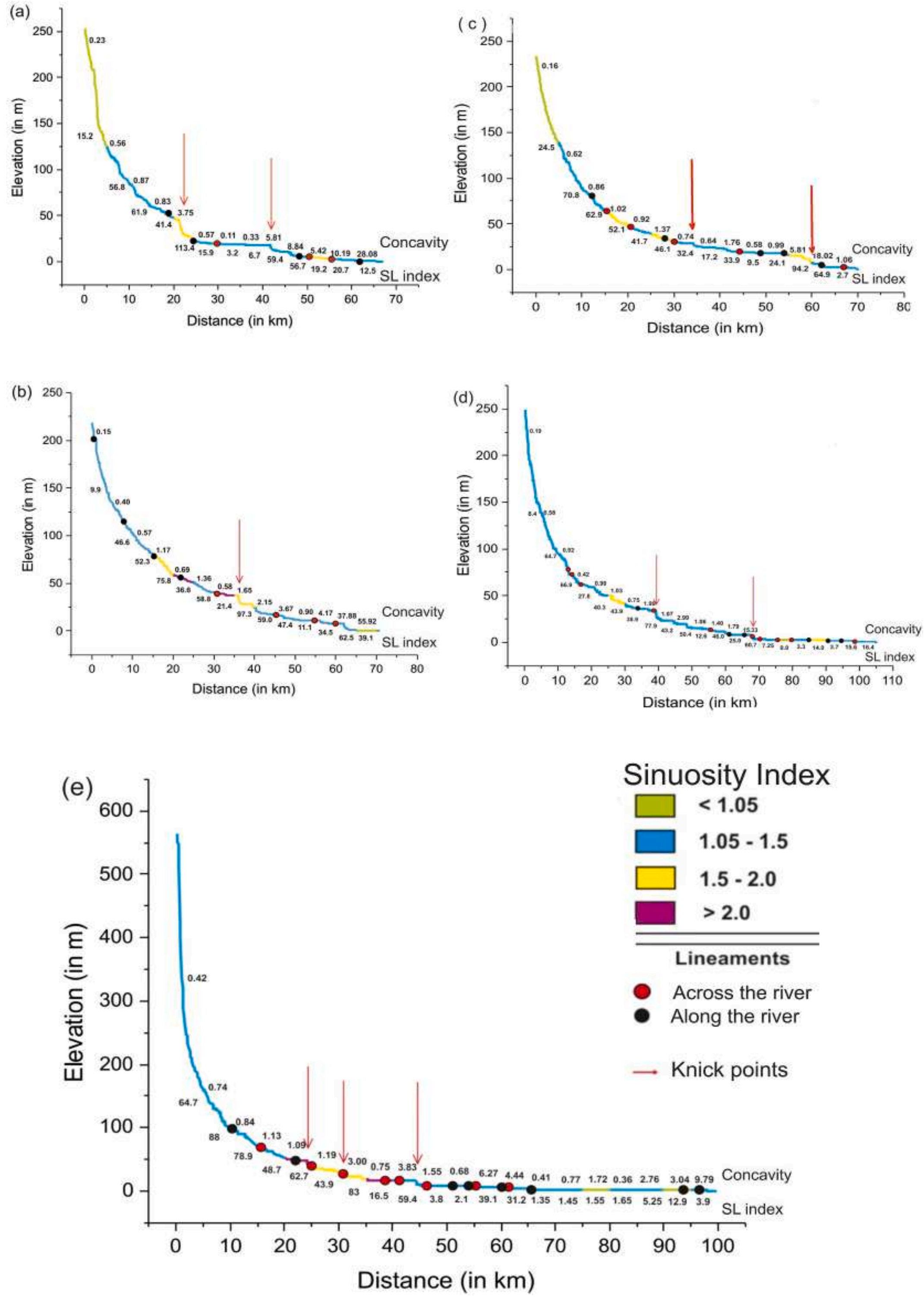

Fig. 4. Linear aspects of morphotectonic features of the five watersheds 1–5 presented as **(a)–(e)**, respectively. Red arrow: anomalies in the curve showing sudden drop in elevation. (For interpretation of the references to colour in this figure legend, the reader is referred to the Web version of this article.)

rectangular areas (Fig. 7). Comparing the spatial distribution of Bouguer anomaly (Figs. 8a-c) with the b-value, it can be observed that regions with less negative Bouguer anomaly (~60 mGal) correspond to the region showing high b-values (~0.9, unitless). A b-value ~1 indicates a tectonically active region (e.g., Joshi et al., 2022). Sections 1 and 4 have higher b values (0.98 and 0.67, respectively; Fig. 9) than those over the overall region. Sections 2 and 3 have lower values. Sections 1 and 4 show fewer negative values of Bouguer anomaly. On the other hand, sections 2 and 3 show more negative Bouguer anomaly values and have b-values of 0.2 and 0.48, respectively. The study area was divided so that the Western Ghats roughly split the region into two halves, with the western part exhibiting a higher b-value than the eastern part.

Section 4 experienced 363 earthquakes from 1967 to 2020 and has a higher b-value than the other sections, indicating lower stress accumulation. However, section 3 also has a high frequency of earthquakes but has the lowest b-value. The highest magnitude reservoir-induced

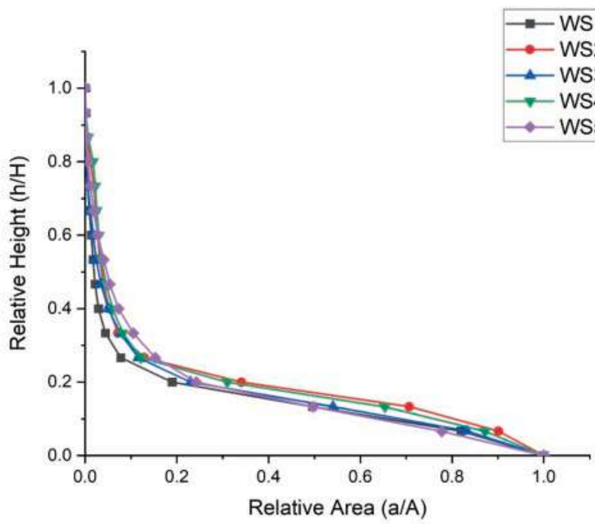

Fig. 5. Hypsometric curves of the five watersheds (WS).

earthquake, magnitude 6.3, occurred in 1967. Despite the energy dissipation through earthquakes, the low b-value indicates high stress accumulation in section 3.

4.4. Gravity modeling results

A regional map of the selected coastal belt was plotted using the WCMI from east to west in the MATLAB 2017 environment, employing the General Bathymetric Chart of the Oceans (GEBCO) bathymetry data (Fig. 10a). This map primarily encompassed the Konkan Coastal Belt (KCB) and the Sahyadri Ranges, with the western boundary defined by the Western Ghats Escarpment (WGE). The east-west trend of deeper features at the crustal scale was evident (Fig. 10). The color bar of the figure illustrated a low bathymetry height around 0 m from mean sea level (MSL) in the Arabian Sea and ~ 1400 m MSL in the Sahyadri Ranges. The north-south trending Sahyadri Ranges paralleled the WCMI, rising to elevations of 1400 m. These ranges were characterized by a steep west-facing escarpment, ranging from 400 to 1200 m, which geologically matched the WGE.

We prepared the FAG (Free-air gravity) map using the EGM2008 data (Fig. 10b). The figure shows a gravity trend varying from ~ −80 mGal to 30 mGal. The offshore area of the study region included basement highs that separated the regional continental shelf into several offshore basins, namely the Kerala-Konkan and Bombay/Mumbai basins. The anomaly map on the western coast along the KCB (Fig. 10b) shows a depressed gravity anomaly up to - 60 mGal, which might indicate the presence of large sedimentary basins in the KCB.

We first estimated the FVD and then the TDR to delineate the edge (boundary) as a lineament with their higher accuracy of spatial occurrence and trend (Fig. 11a and b). The delineated lineaments studied using FVD and TDR illustrated the edge extensions (black lines) of the relevant sources that could be related to basement (sedimentary) fault blocks, fractures, shear zones, and lithological contacts (Kumar et al., 2022). The lineament diagrams were identified from edge-enhanced maps, and respective plots with their strikes (black lines) were plotted (Fig. 11a and b). These lineament plots revealed the trend of the major structural features. The lineaments diagram plotted by using the FVD technique shows that the structural fabrics mostly trend ~ NW-SE in the west of WGE while NE-SW at the east (Fig. 11a).

The lineament diagram plotted using the TDR technique exhibited a major NE-SW trend to the west of the WGE, while an E-W trend was observed in the eastern part (Fig. 11b). These trends revealed a parallel trend of the faults of Indian western coast (Das and Ray, 1976) supporting our analysis using FVD and TDR techniques. The Dharwar trends intersected the western Indian continent in many places as NE-SW trending lineaments (Ramana, 1986). In the north, the NE-SW Aravalli trend, and in the south, the NE-SW Western Ghat trend is the dominant structural fabrics. In western India, the other dominant ENE-WSW trend is known as the Satpura trend. These main tectonic trends control the tectonic structure of several pericratonic and intracratonic western Indian sedimentary basins (Bullen et al., 2003; Biswas, 1987).

Morphometric investigations together with seismic and gravity models revealed that all the studied watersheds are tectonically active. The linear and watershed scale indicators support the geophysical investigations that show a strong correlation between river courses and lineaments predicted by TDR and FVD. The kick points along the master streams define structural controls on the channels where lineaments exist across and along the channels. The lineament diagrams were identified from edge-enhanced maps.

These lineaments trend (sub)parallel to the active faults on the west coast. These results help to understand the active geologic features at a regional scale.

Table 1
R^2 value of exponential, linear, logarithmic and power relations for best fit curves. For the watersheds 1, 2 and 3, the logarithmic trend-line shows the maximum values. For watersheds 4 and 5, the highest values fit the exponential curve.

	Watershed 1	Watershed 2	Watershed 3	Watershed 4	Watershed 5
Exponential	0.9192	0.8015	0.8739	0.9839	0.9482
Linear	0.6631	0.8244	0.7084	0.6626	0.4388
Logarithmic	0.967	0.9766	0.9748	0.9784	0.8767
Power	0.6617	0.5351	0.6574	0.7615	0.8669

Table 2
Values of the areal aspects of the morphotectonic analysis.

Watersheds	Hypsometric Integral (HI, unitless)	Asymmetry Factor (AF, unitless)	Mountain front sinuosity (S_{mf}, unitless)	Drainage Texture R_t (m^{-1})	Drainage density D (m^{-1})	Basin shape index (B_s) (unitless)
1	0.14853	63.25	2.59	0.336703	0.361	3.093894
2	0.19068	57.19	2.55	0.363222	0.347	2.308704
3	0.16271	40.19	1.49	0.269114	0.332	2.804382
4	0.18523	79.29	1.25	0.719126	0.356	1.845287
5	0.16698	37.14	1.15	0.756995	0.363	1.2251

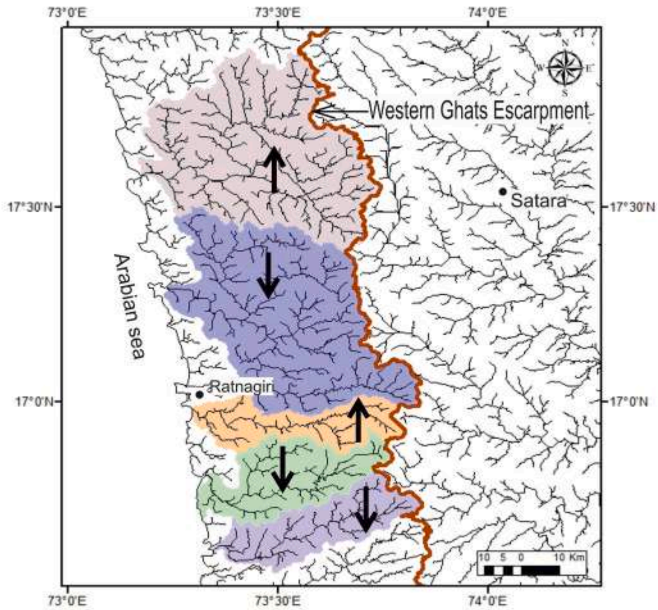

Fig. 6. Tilt direction of the five watersheds as per the Asymmetry Factor (AF). Black arrow: direction towards which the watersheds are tilted.

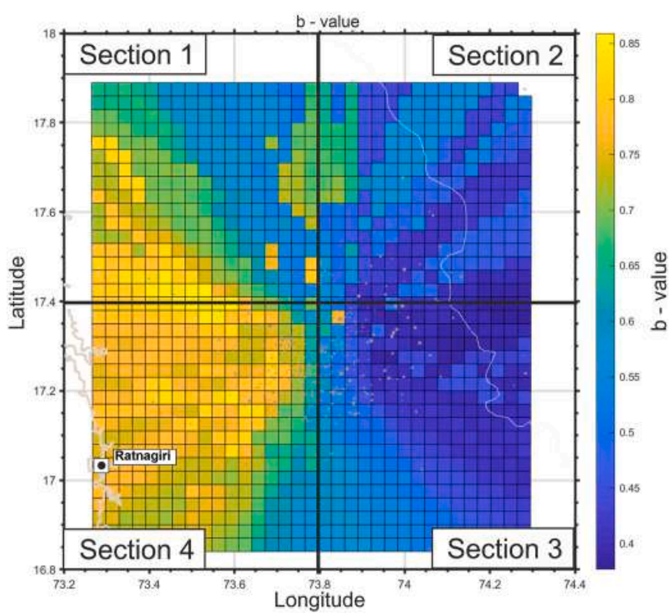

Fig. 7. Spatial variation in b-values in sections 1-4. See Repository Fig. 3 for the different watersheds that come under these sections.

5. Discussions

5.1. Stress axes and lineaments

The azimuth and plunge data of the maximum horizontal stress direction (S_H) obtained from the WSM indicates that the study area falls under a normal and strike-slip regime. S_H trends ~ NW-SE. This implies that the minimum horizontal stress axis (S_h) trends ~ NE-SW. This is consistent with the NE-SW extension caused by the rifting of the Indian landmass from Madagascar that started ~90 Ma ago. The lineaments in this region also trend NW-SE (Nagarajan et al., 2000; Dixit et al., 2014; Arora and Srinu, 2022; Repository Fig. 1), which is consistent with the faulting due to separation/extension. The NW trend of lineaments is reflected in the overall drainage pattern as well. Owing to the presence of a number of lineaments, the tributaries show straight courses, right-angle bends, and parallel streams, mostly from watersheds 4 and 5. In watershed 5, a few south-flowing tributaries join the west-flowing main channels at right angles following the lineaments.

5.2. Geomorphology

A rectangular drainage pattern indicated tectonic control of the terrain. While the main river channels show a more mature stage, the tributaries remain ungraded (Dikshit et al., 2000). The study area also hosts several thermal springs aligned N-S, suggesting that shallow crustal tectonics might have been active in the region at present (Jain et al., 2020). This supports the recent work by Goswami et al. (2024) that indicated shallow (<10 km) seismicity in the Koyna region.

The effect of the lineaments on the sinuosity of the river channels can be described from the sinuosity values of the stream segments. When a river flows along a straight path, it can be due to the following reasons. *(i)* It flows along a pre-existing lineament. *(ii)* It has encountered a region undergoing uplift and cuts across the rock bed to regain equilibrium. *(iii)* It flows straight over a uniform lithology. Uplift changes the sinuosity of rivers to maintain its equilibrium. The river becomes straighter in the region of tectonic instability and becomes more sinuous in the region surrounding it. From the graphs of SI (Fig. 4), it is observed that for all watersheds except the third one, a drop in the SI is accompanied by an increase in the values in the adjacent segments. This indicates the presence of uplift or any lineament that crosses the river channel. For instance, in Watershed 5, a similar lineament and stream course trend is seen (Fig. 1) where the Chiplun Lineament passes. In the rest of the cases, a low SI value may indicate a high gradient of the escarpment or due to the flow of the river along a lineament.

As per the AF values, watershed 4 is tilted significantly, followed by the watersheds 1 and 5. Watersheds 2 and 3 are quite symmetric and show little difference between the areas across the main river channel. In watershed 4, the area towards the north of the main river channel is significantly higher than that towards the south, indicating that there might be a southward tilt. However, the adjacent watershed 5 shows AF < 50, indicating it might be tilted towards the north. This can be explained by a N-S trending drainage divide between the two watersheds. Watershed 3 is also tilted towards the south. This alternation of tilt direction might indicate the presence of culmination and depression in the region. Although the asymmetry of a river basin can be ascribed to tectonic tilting, it may also of result from variable lithology, steep slopes, climatic factors, and the presence of lineaments. Drainage texture (Rt) analysis correlates with the distribution of the grains carried by the rivers (Rai et al., 2019). It is related to the flow velocity, steep gradient and shear stress of the rivers. Watersheds 4 and 5 show significantly higher values of Rt, 0.719126 and 0.756995, respectively. Drainage densities of five watersheds indicate that tributaries are widened over the study area. Drainage lines in watersheds 4 and 5 are mostly controlled by lineaments that produce several major channels. The B_s values are lower in watersheds 4 and 5, 1.845287 and 1.2251, respectively (Table 2).

Sigmoid hypsometric curves possess low magnitudes of HIs. This is due to a very high gradient near the escarpment and abrupt change in slope as the river reaches the Konkan plain. HI for the river Jaigad in watershed 4 is higher than the other watersheds. This indicates that the river is in a youthful stage and the watershed is tectonically active.

The concavity index of all the watersheds is low, indicating the unstable areas. The longitudinal profile curves of most rivers show a sharp drop in elevation, corresponding to the knick-points. This indicates that a sudden drop in the elevation occurred along the course of the river. This can be caused due to tectonic uplift and the resulting down-cutting of the bedrock. However, other factors need to be considered. A sudden drop in elevation could also be due to a variation in lithology or the presence of a dam or a waterfall. This can make the knick points

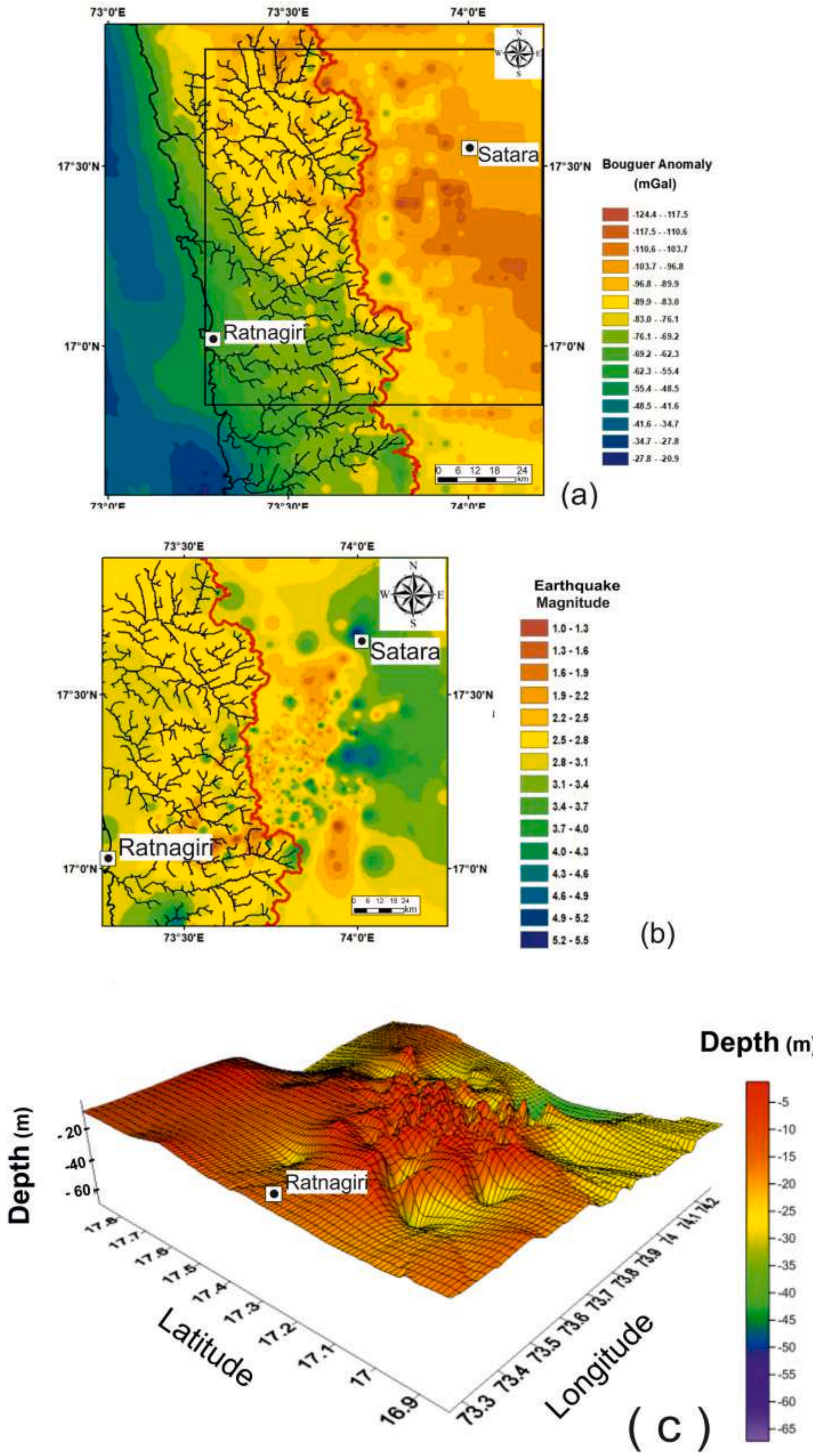

Fig. 8. **a**. Bouguer anomaly map of study area (data from EGM2008). **b.** Earthquake magnitude distribution in the black rectangular region of Fig. 8a. **c.** Hypocenter depth distribution.

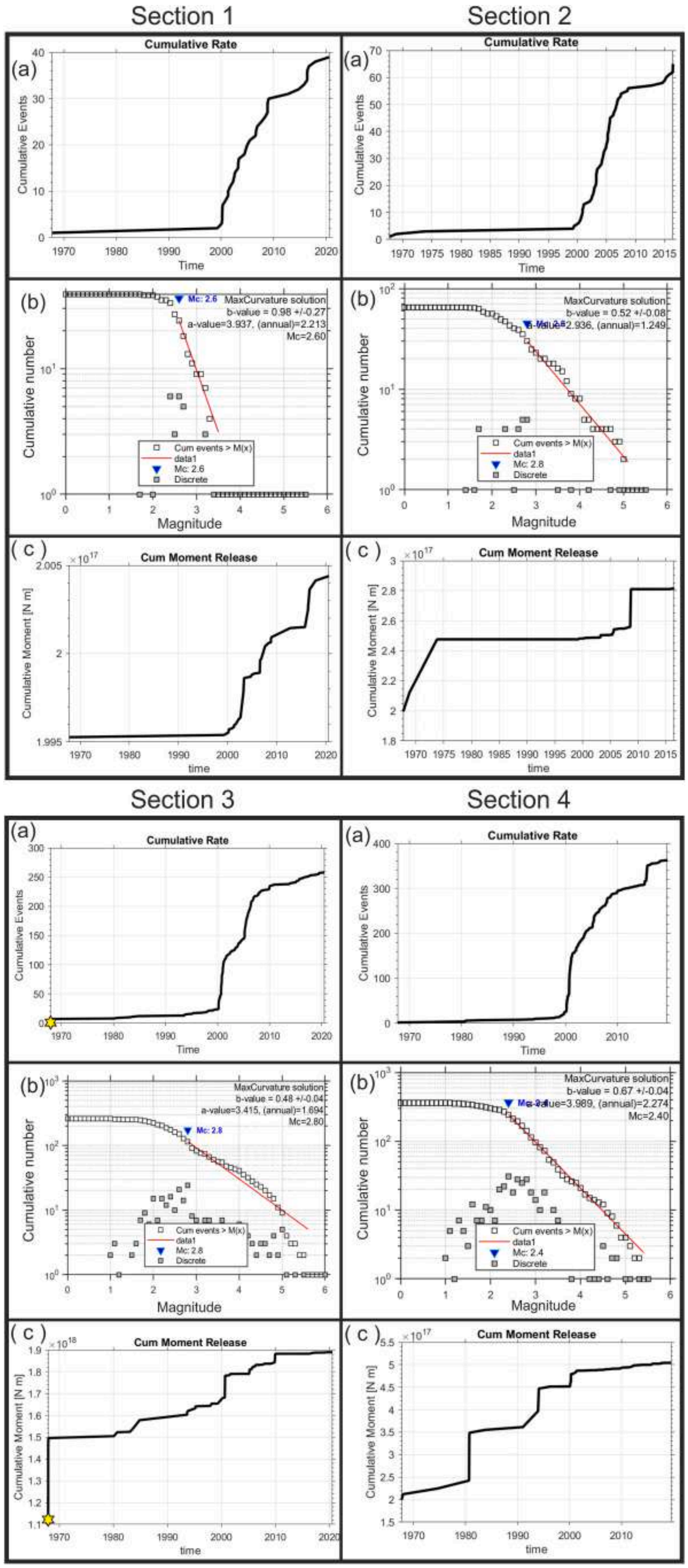

Fig. 9. In regions 1–4. **(a)** Temporal variation in cumulative number of seismic events. **(b)** Frequency-magnitude distribution (Gutenberg-Richter Relation). **(c)** Temporal variation in a cumulative moment (in Nm).

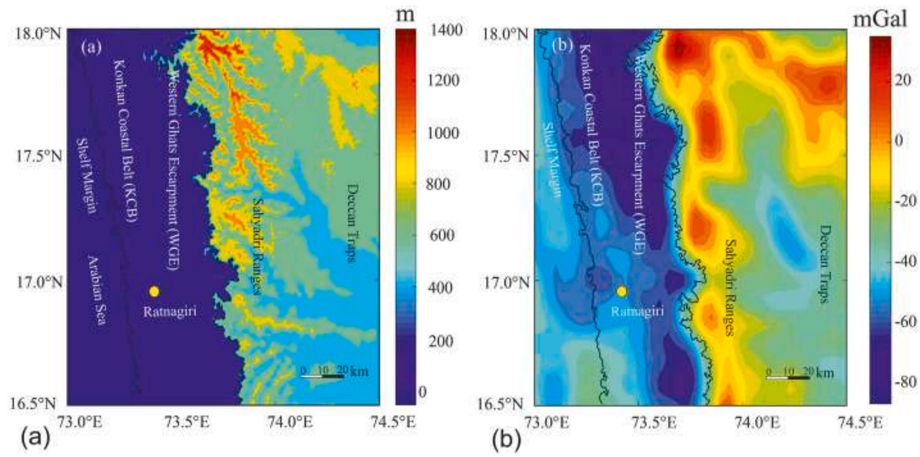

Fig. 10. a. The Regional map of the selected area along with the western continental margin of India (WCMI) has been plotted by using GEBCO bathymetry data (www.gebco.net/data_and_products). Color bar: mean sea level (MSL), height in m. Repository Fig. 4 presents a superposition between this map and the watershed map. b. Regional FAG map of the selected area along with the WCMI. Color bar: gravity trend (mGal). Repository Fig. 5 presents a superposition between this map and the watershed map. (For interpretation of the references to colour in this figure legend, the reader is referred to the Web version of this article.)

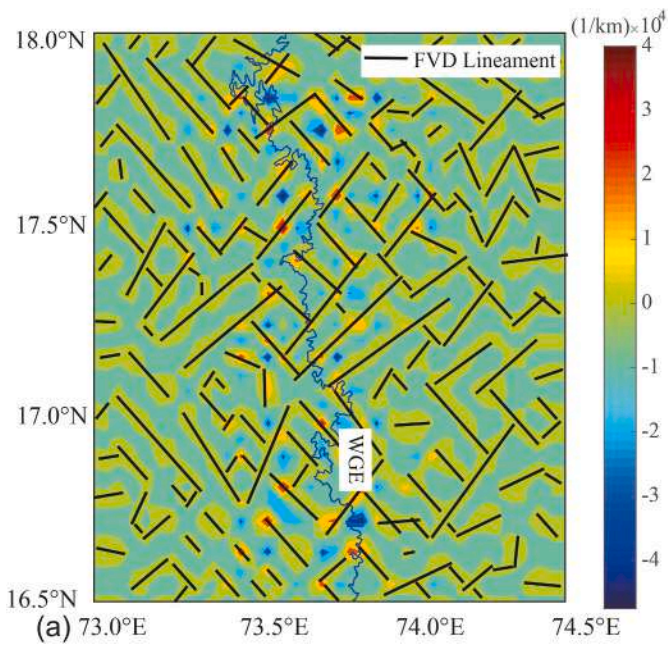

Fig. 11a. The delineated lineaments estimated by First vertical derivative (FVD) with edge extension (black lines). Color bar: FVD amplitude of gravity anomaly in (km^{-1}) $\times$ 10^4. (For interpretation of the references to colour in this figure legend, the reader is referred to the Web version of this article.)

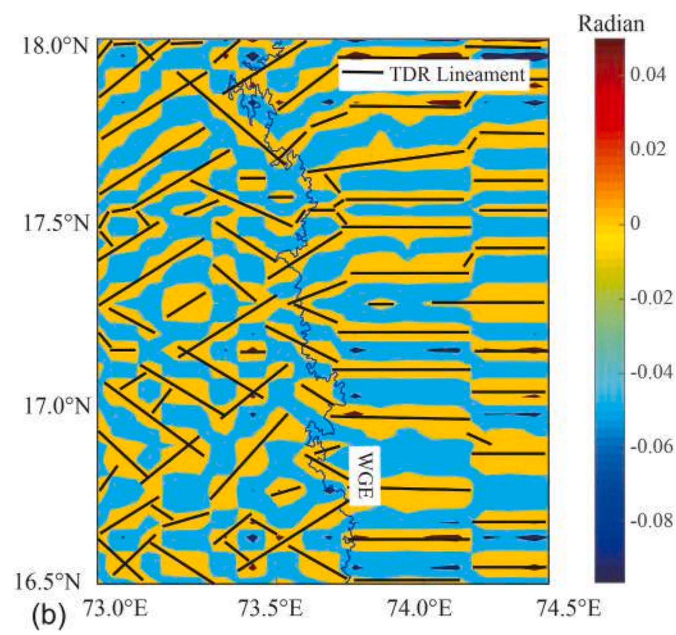

Fig. 11b. Delineated lineaments estimated by TDR with edge extension (black lines). Color bar: TDR amplitude in radian. Repository Fig. 6 presents a superposition between this map and the watershed map. (For interpretation of the references to colour in this figure legend, the reader is referred to the Web version of this article.)

unreliable in commenting about tectonic activity to some extent, and fieldwork would be required for confirmation. Field evidence, viz., triangular facets, river terraces, drainage offset and sharp escarpments may indicate the presence of tectonic activity.

As evident from the longitudinal profile analysis, watersheds 1–3 are moderately active tectonically, while watersheds 4 and 5 are highly active. This is also corroborated by the Smf values of the watersheds, where watersheds 4 and 5 show the lowest values, indicating that they are more active. One expects thermal springs, if any, close to the tectonically active terrains. This is corroborated by a greater number of thermal springs in watershed 4 located ~ SW of Koyna (Repository Fig. 1).

5.3. Geophysical aspects

The earthquake data map shows that seismicity concentrates near the Koyna-Warna Lineament zone, located east of the Western Ghats escarpment, on the uplands. The zone is located near the watersheds 4 and 5. The origin of these earthquakes has been ascribed to reservoir-induced seismicity due to the presence of the Koyna reservoir (Yadav et al., 2016). However, ~30 earthquake foci are located on the Konkan plain, far away from the uplands. These could be due to probable blind faults and their reactivation enhanced by the reservoir-induced seismicity. As per Pandey and Chadha (2003), the subsurface fracture network affected the local tectonic activity and could be a factor that triggers seismicity in the Koyna-Warna region. However, zones of active tectonics need not always be seismic (Allen et al., 1965; Castro et al., 2017).

The b-value parameter continues to be one of the most applied methods of inferring the stress conditions in different terrains (e.g., Gadkari and Mukherjee, 2023). The tectonic activity in watersheds 4 and 5 can be attributed to the presence of a region with low b-values near the source of the rivers. Although rivers flow through Sections 1 and 4 (Fig. 8), they originate close to watersheds 2 and 3, which have very low Bouguer anomaly (~−90 mGal) and low b-values (~0.5). This is attributed to the fact that the region lies on the Koyna-Warna Lineament zone and is susceptible to reservoir-induced seismicity. The area with low b-values lies close to watersheds 4 and 5 and is the most tectonically active at present.

The July 2021 landslide data plotted in Fig. 1 shows that the majority of the slides took place in and around watersheds 4 and 5 (Fig. 1). Watershed 4 hosts a landslide-prone zone. Although other factors affect landslide susceptibility, the data tentatively confirm the presence of ongoing tectonic activity in watersheds 4 and 5.

Gravity study-derived lineaments (Figs. 12 and 13) show a broader trend than those reported by previous authors based on remote sensing image interpretation (Repository Fig. 1). This inconsistency can be studied in detail by mapping geophysically the sub-surface structures.

6. Conclusions

The structural orientation of the Konkan plain trends ~ NW-SE. Major stream courses are lineament-controlled. Morpho- and seismo-tectonic analyses, recent landslide data, low Bouguer gravity values and hot spring locations indicate that watersheds 4 and 5 are more tectonically active and are characterized by a higher hypsometric integral. Wells drilled for exploration for hydrocarbon or for other purposes, such as borehole observatories in and around these two watersheds, must plan well-bore stability issues in advance.

Using the FVD technique, the lineament plots reveal that the structural fabrics mostly trend ~ NW-SE in the west of WGE while NE-SW at the east. The lineament plots using the TDR technique display a major NE-SW trend at the west of WGE, while an E-W trend at the eastern part is seen at the west of WGE. These trends reveal a parallel trend of faults of the Indian western coast and support the current analysis of FVD and TDR techniques. The Dharwar trends intersected the western Indian continent at several places as NE-SW trending lineaments. Thus, the NE-SW Aravalli trend in the north and the NE-SW Western Ghat trend in the south are the dominant structural fabrics. Gravity and remote sensing image-derived lineaments do not show a uniform pattern. Geophysical studies targeting deep crust, structural geological fieldworks, and drill-core interpretations would, therefore, be required to get a more coherent structural scenario of the area.

CRediT authorship contribution statement

Shatavisa Chatterjee: Investigation, Formal analysis. Kutubuddin Ansari: Formal analysis. Mery Biswas: Formal analysis. Soumyajit Mukherjee: Writing – review & editing, Supervision, Conceptualization. B. Kavitha: Preparation of supplementary files

Declaration of competing interest

The authors declare that they have no known competing financial interests or personal relationships that could have appeared to influence the work reported in this paper.

Acknowledgements

This work was performed as an M.Sc. thesis of SC under SM. No funding was received. We thank Ana Luiza Spadano Albuquerque (Chief Editor), Gabriel Nuto Nóbrega (Section Editor) and two anonymous reviewers for providing detail comments. Adrija Raha (Presidency University, Kolkata) provided guided SC in the lab. Megh Kanvinde (IIT Bombay) provided minor assistance with figures.

Appendix A. Supplementary data

Supplementary data to this article can be found online at https://doi.org/10.1016/j.eve.2024.100041.

Data availability

Data will be made available on request.

References

Allen, C.R., Amand, P.S., Richter, C.F., Nordquist, J.M., 1965. Relation between seismicity and geological structure in the southern California region. Seismol. Soc. Am. Bull. 55, 752–797.
Arora, K., Srinu, Y., 2021. Morphometric analysis of koyna-warna region seismicity. J. Geol. Soc. India 97, 1583–1589.
Arora, K., Srinu, Y., 2022. Surface traces of seismogenic faults from airborne LiDAR in koyna–warna region of deccan volcanic province. J. Earth Syst. Sci. 131, 1–9.
Baratin, L.M., Mazzotti, S., Chéry, J., Vernant, P., Tahayt, A., Mourabit, T., 2016. Incipient mantle delamination, active tectonics and crustal thickening in Northern Morocco: insights from gravity data and numerical modeling. Earth Planet Sci. Lett. 454, 113–120.
Bayasgalan, A., Jackson, J., McKenzie, D., 2005. Lithosphere rheology and active tectonics in Mongolia: relations between earthquake source parameters, gravity and GPS measurements. Geophys. J. Int. 163, 1151–1179.
Beane, J.E., Turner, C.A., Hooper, P.R., Subbarao, K.V., Walsh, J.N., 1986. Stratigraphy, composition and form of the deccan basalts, western Ghats, India. Bull. Volcanol. 48, 61–83.
Biswas, M., Mukherjee, S., Gogoi, M.P., Barik, N., 2024. Assessment of Active Tectonics of the Tripura-Mizoram Fold Belt (Surma Basin), North East India.
Bhave, N., Imran Siddique, M., Desai, J., Pillai, S.P., Dole, G., Kulkarni, H., Kale, V.S., 2017. Faulting in Deccan traps in the vicinity of Koyna-Warna Seismic Zone. J. Geological Soc. India 90, 748–751.
Biswas, S.K., 1987. Regional tectonic framework, structure and evolution of the western marginal basins of India. Tectonophysics 135, 307–327.
Biswas, M, Puniya, MK, Gogoi, MP, Dasgupta, S, Mukherjee, S, Kar, NR, 2022. Morphotectonic analysis of petroliferous Barmer rift basin (Rajasthan, India). Journal of Earth System Science 131, 140.
Borah, U.K., Patro, P.K., Reddy, K.C., Babu, N., 2023. Deccan trap configuration in and around koyna-warna seismic zone, India: a magnetotelluric approach. J. Appl. Geophys. 208, 104875.
Bullen, M.E., Burbank, D.W., Garver, J.I., 2003. Building the northern Tien Shan: integrated thermal, structural, and topographic constraints. J. Geol. 111, 149–165.
Castro, R.R., Stock, J.M., Hauksson, E., Clayton, R.W., 2017. Active tectonics in the Gulf of California and seismicity (M> 3.0) for the period 2002–2014. Tectonophysics 719, 4–16.
Cheng, K.Y., Hung, J.H., Chang, H.C., Tsai, H., Sung, Q.C., 2012. Scale independence of basin hypsometry and steady state topography. Geomorphology 171, 1–11.
Das, S.R., Ray, A.K., 1976. Fracture pattern, hot springs and lineaments of the west coast. Geol. Surv. Ind. 125, 1–6.
Dasgupta, Biswas M., Mukherjee, S., Chatterjee, R., 2022. Structural evolution and sediment depositional system along the transform margin- Palar-Pennar basin, Indian east coast. J. Petrol. Sci. Eng. 211, 110155.
Dessai, A.G., Bertrand, H., 1995. The "Panvel Flexure" along the Western Indian continental margin: an extensional fault structure related to Deccan magmatism. Tectonophysics 241, 165–178.
Dikshit, K.R., 1976. Drainage basins of konkan: forms and characteristics. Natl. Geogr. J. India 22, 79–105.
Dixit, M.M., Kumar, S., Catchings, R.D., Suman, K., Sarkar, D., Sen, M.K., 2014. Seismicity, faulting, and structure of the Koyna-Warna seismic region, Western India from local earthquake tomography and hypocenter locations. J. Geophys. Res. Solid Earth 119, 6372–6398.
Dwivedi, A.K., 2016. Petroleum exploration in India - a perspective and endeavours. Proc Indian Nat Sci Acad 82, 881–903.
Evjen, H.M., 1936. The place of the vertical gradient in gravitational interpretations. Geophysics 1, 127–136.
Gadkari, D., Mukherjee, S., 2023. Assessment of efficacy of "b" value as a seismic precursor for select major seismic events. In: Mukherjee, S., Dasgupta, S., Majumdar, C., Mondal, S., Dasgupta, T. (Eds.), Handbook of Petroleum Geoscience: Exploration, Characterization, and Exploitation of Hydrocarbon Reservoirs. Wiley, pp. 413–427.
Gailleton, B., Mudd, S.M., Clubb, F.J., Grieve, S.W., Hurst, M.D., 2021. Impact of changing concavity indices on channel steepness and divide migration metrics. J. Geophys. Res.: Earth Surf. 126. https://doi.org/10.1029/2020JF006060.
Ganguli, S.S., Singh, S., Das, N., Maurya, D., Pal, S.K., Rama Rao, J.V., 2019. Gravity and magnetic survey in southwestern part of Cuddapah Basin, India and its implication for shallow crustal architecture and mineralization. J. Geol. Soc. India 93, 419–430.
Gogoi, M.P., Gogoi, B., Mukherjee, S., 2022. Tectonic instability of the petroliferous upper Assam valley (NE India): a geomorphic approach. J. Earth Syst. Sci. 131, 18.

Goswami, D., Akkiraju, V.V., Roy, S., 2024. Heat flow and thermal structure in the Koyna seismic zone, western India: implications for recurrent reservoir triggered seismicity. Tectonophysics 873, 230216.
Gunnell, Y., Fleitout, L., 2000. The morphotectonic evolution of the Wetsren Ghats, India: an exploration of denudation-driven flexural models. In: Summerfield, M.A. (Ed.), Geomorphology and Global Tectonics. John Wiley and Sons, pp. 321–338.
Gupta, S., Biswas, M., 2023. Seismo-tectonic and morphological study of the north-east Himalaya. Geosci. J. 27, 1–21.
Heidbach, O., Rajabi, M., Reiter, K., Ziegler, M., 2019. World stress map. In: Sorkhabhi, R. (Ed.), Encyclopedia of Petroleum Geoscience. Springer, pp. 1–8. https://doi.org/10.1007/978-3-319-02330-4.
Hirata, T., 1989. A correlation between the b value and the fractal dimension of earthquakes. J. Geophys. Res. Solid Earth 94, 7507–7514.
Horton, R.E., 1932. Drainage basin characteristics. Trans. Am. Geophys. Union 13, 350–361.
Horton, R.E., 1945. Erosional development of streams and their drainage basins: hydrophysical approach to quantitative morphology. Geol. Soc. Am. Bull. 56, 275–370.
Horo, D., Pal, S.K., Singh, S., Srivastava, S., 2020. Combined self-potential, electrical resistivity tomography and induced polarisation for mapping of gold prospective zones over a part of Babaikundi-Birgaon Axis, North Singhbhum Mobile Belt, India. Explor. Geophys. 51, 507–522.
Internet ref-1. https://ndma.gov.in/sites/default/files/PDF/Landslide/NLRMS.pdf. (Accessed 20 July 2024).
Internet ref-2: URL: bhuvan.nrsc.Gov.in (Accessed on 18-July-2024).
Iwata, D., Nanjo, K.Z., 2024. Adaptive estimation of the Gutenberg–Richter b value using a state space model and particle filtering. Sci. Rep. 14, 4630.
Jadhav, P.B., Kshirsagar, L.K., 2017. Tectonic geomorphology in parts of Koyna region, Maharashtra. J. Geol. Soc. India 90, 738–741.
Jain, A.K., Banerjee, D.M., Kale, V.S., 2020. Tectonics of the Indian Subcontinent. Springer Nature.
Joshi, M., Kothyari, G.C., Malik, K., Taloor, A.K., 2022. Response of drainage to tectonics and PS-InSAR derived deformation study in Bilaspur, northwestern Himalaya, India. Geodesy Geodyn 13, 205–218.
Kale, V.S., Dole, G., Upasani, D., Pillai, S.P., 2017. Deccan Plateau uplift: insights from parts of western uplands, Maharashtra, India. In: Mukherjee, S. (Ed.), Tectonics of the Deccan Large Igneous Province, vol. 445. Spec. Publ., Geol. Soc., London, pp. 11–46.
Kannaujiya, et al., 2022. Unraveling seismic hazard by estimating prolonged crustal strain buildup in Kumaun-Garhwal, Northwest Himalaya using GPS measurements. J. Asian Earth Sci. 223, 104993.
Keller, E.A., 1986. Investigation of active tectonics: use of surficial earth processes. Active Tectonics 1, 136–147.
Keller, E.A., Pinter, N., 1996. Active, Tectonics: Earthquake, Uplift and Landscape. Prentice Hall Publication.
Keller, E.A., Pinter, N., 2002. Active Tectonics: Earthquakes, Uplift and Landscapes, second ed. Prentice Hall, Upper Saddle River.
Kumar, N., 2018. Petroleum potential of the West Coast of India. J. Ind. Assoc. Sedimentol. 35, 33–49.
Kumar, U., Narayan, S., Pal, S.K., 2022. Structural and tectonic interpretation of EGM2008 gravity data around the Laccadive ridge in the Western Indian Ocean: an implication to continental crust. Geocarto Int. 37, 3179–3198.
Kumar, U., Pal, S.K., Sahoo, S.D., Narayan, S., Mondal, S., Ganguli, S.S., 2018. Lineament mapping over Sir Creek offshore and its surroundings using high resolution EGM2008 Gravity data: an integrated derivative approach. J. Geol. Soc. India 91, 671–678.
Kundu, B., Matam, A., 2000. Identification of probable faults in the vicinity of Harnai–Ratnagiri region of the Konkan coast, Maharashtra, India. Curr. Sci. 78, 1556–1560.
Lavecchia, G., Nardis, R.D., Ferrarini, F., Cirillo, D., Bello, S., Brozzetti, F., 2021. Regional seismotectonic zonation of hydrocarbon fields in active thrust belts: a case study from Italy. In: Bonali, F.L., Mariotto, F.P., Tsereteli, N. (Eds.), Building Knowledge for Geohazard Assessment and Management in the Caucasus and Other Orogenic Regions. Springer, Dordrecht, pp. 89–128.
Lee, C.S., Tsai, L.L., 2010. A quantitative analysis for geomorphic indices of longitudinal river profile: a case study of the Choushui River, Central Taiwan. Env. Earth Sci. 59, 1549–1558.
Martha, T.R., Roy, P., Jain, N., Khanna, K., Mrinalni, K., Kumar, K.V., Rao, P.V.N., 2021. Geospatial landslide inventory of India—an insight into occurrence and exposure on a national scale. Landslides 18, 2125–2141.
Miller, H.G., Singh, V., 1994. Potential field tilt—a new concept for location of potential field sources. J. Appl. Geophys. 32, 213–217.
Modak, K., 2024. Evidence of water percolation in granitoid basement in Koyna seismogenic zone: implications for reservoir triggered seismicity. J. Earth Syst. Sci. 133, 1–18.
Modak, K., Rohilla, S., Podugu, N., Goswami, D., Roy, S., 2022. Fault associated with the 1967 M 6.3 Koyna earthquake, India: a review of recent studies and perspectives for further probing. J. Asian Earth Sci. X, 100123.
Mukherjee, S., Dole, G., Yatheesh, V., Kale, V.S., 2020. Tectonics of the deccan trap: focus on Indian geoscientists' contribution in the last four years. Proc. Ind. Nat. Sci. Acad. 86, 237–244.
Mukherjee, S., Misra, A.A., Calvès, G., Nemčok, M., 2017. Tectonics of the Deccan large igneous province: an introduction. In: Mukherjee, S., Misra, A.A., Calvès, G., Nemčok, M. (Eds.), Tectonics of the Deccan Large Igneous Province, vol. 445. Spec. Publ., Geol. Soc., London, pp. 1–9.
Nagarajan, R., Roy, A., Vinod Kumar, R., Mukherjee, A., Khire, M.V., 2000. Landslide hazard susceptibility mapping based on terrain and climatic factors for tropical monsoon regions. Bull. Eng. Geol. Environ. 58, 275–287.
Narayan, S., Sahoo, S.D., Pal, S.K., Kumar, U., Pathak, V.K., Majumdar, T.J., Chouhan, A., 2017. Delineation of structural features over a part of the Bay of Bengal using total and balanced horizontal derivative techniques. Geocarto Int. 32, 351–366.
National Landslide Risk Management Strategy, 2019. A Publication of the National Disaster Management Authority. Government of India, New Delhi.
Pal, S.K., Majumdar, T.J., Pathak, V.K., Narayan, S., Kumar, U., Goswami, O.P., 2016. Utilization of high-resolution EGM2008 gravity data for geological exploration over the Singhbhum-Orissa Craton, India. Geocarto Int. 31, 783–802.
Pandey, A.P., Chadha, R.K., 2003. Surface loading and triggered earthquakes in the Koyna–Warna region, western India. Phys. Earth Planet. In. 139, 207–223.
Podugu, N., Goswami, D., Akkiraju, V.V., Roy, S., 2023. In-situ physical and elastic properties of Archaean basement granitoids in the Koyna seismogenic zone, western India from 3 km downhole geophysical well logs: implications for water percolation at depth. Tectonophysics 848, 229725.
Radhakrishna, B.P., 1993. Neogene uplift and geomorphic rejuvenation of the Indian Peninsula. Curr. Sci. 64, 787–793.
Rai, P.K., Singh, P., Mishra, V.N., Singh, A., Sajan, B., Shahi, A.P., 2019. Geospatial approach for quantitative drainage morphometric analysis of Varuna river basin, India. J. Landscape Ecol. 12, 1–25.
Rai, S.S., Singh, S.K., Sarma, P.V.S.S., Srinagesh, D., Reddy, K.N.S., Prakasam, K.S., Satyanarayana, Y., 1999. What triggers Koyna region earthquakes? Preliminary results from seismic tomography digital array. Proc. Ind. Acad. Sci.-Earth Planet. Sci. 108, 1–14.
Rajaram, C., Narender, B., Satyam, N.D., Kumar, P.R., 2010. Preliminary Seismic Hazard Map of Peninsular India.
Rajaram, M., Anand, S.P., Erram, V.C., Shinde, B.N., 2017. Insight into the structures below the Deccan Trap-covered region of Maharashtra, India from geopotential data. In: Mukherjee, S., Misra, A.A., Calvès, G., Nemčok, M. (Eds.), Tectonics of the Deccan Large Igneous Province, vol. 445. Spec. Publ., Geol. Soc., London, pp. 219–236.
Ramana, M.V., 1986. Regional tectonic trends on the inner continental shelf off Konkan and central west coast of India. Geo Mar. Lett. 6, 1–5.
Ray, L., Gupta, R.K., Chopra, N., Gopinadh, D., Dwivedi, S.K., 2021. Thermal and physical properties of Deccan basalt and Neoarchean basement cores from a deep scientific borehole in the Koyna– Warna seismogenic region, Deccan Volcanic Province, western India: Implications on thermal modeling and seismogenesis. Earth Space Sci. 8, e2021EA001645.
Rehman, K., Ali, A., Ahmed, S., Ali, W., Ali, A., Khan, M.Y., 2015. Spatio-temporal variations of b-value in and around north Pakistan. J. Earth Syst. Sci. 124, 1445–1456.
Roy, S.K., Shashidhar, D., 2023. Spatial variation in the crustal deformation pattern in the Koyna-Warna region, western India using shear wave splitting. Geophys. J. Int. 235, 1339–1352.
Schumm, S.A., 1956. The evolution of drainage systems and slopes in bad lands at Perth, Amboi, New Jersey. Geol. Soc. Am. Bull. 67, 597–646.
Shekar, P.R., Mathew, A., 2024. Morphometric analysis of watersheds: a comprehensive review of data sources, quality, and geospatial techniques. Watershed Ecol. Env. 6, 13–25.
Shekar, M., Subhadra, N., Srinagesh, D., 2023. Coda Q from educational seismograph network around Koyna–Warna, western India. J. Earth Syst. Sci. 132, 98.
Sheth, H.C., 2007. Large Igneous Provinces (LIPs)': definition, recommended terminology, and a hierarchical classification. Earth Sci. Rev. 85, 117–124.
Singh, C., Bhattacharya, P.M., Chadha, R.K., 2008. Seismicity in the Koyna–Warna reservoir site in Western India: fractal and b-value mapping. Bull. Seismol. Soc. Am. 98, 476–482.
Singh, N.K., Lal, N.K., 2001. Geology and petroleum prospects of the Konkan-Kerala basin. Mem. Geol. Soc Ind, 393–402.
Smith, K.G., 1950. Standards for grading textures of erosional topography. Am. J. Sci. 48, 655–668.
Vanik, N., Shaikh, H., Mukherjee, S., Maurya, D.M., Chamyal, L.S., 2018. Post-Deccan trap stress reorientation under transpression: evidence from fault slip analyses from SW Saurashtra, western India. J. Geodyn. 121, 9–19.
Widdowson, M., Cox, K.G., 1996. Uplift and erosional history of the deccan traps, India: evidence from laterites and drainage patterns of the western Ghats and konkan coast. Earth Planet Sci. Lett. 137, 57–69.
Wiemer, S., 2001. A software package to analyze seismicity: zmap. Seismol Res. Lett. 72, 373–382.
Wu, H., Li, L., Xing, C., Zhang, S., 2017. A new method of edge detection based on the total horizontal derivative and the modulus of full tensor gravity gradient. J. Appl. Geophys. 139, 239–245.
Yadav, A., Bansal, B.K., Pandey, A.P., 2016. Five decades of triggered earthquakes in Koyna-Warna region, western India–a review. Earth Sci. Rev. 162, 433–450.